Journal of Power Sources 226 (2013) 340–345

Contents lists available at SciVerse ScienceDirect

Journal of Power Sources

journal homepage: www.elsevier.com/locate/jpowsour

Fabrication and electrochemical properties of $LiMn_2O_4/SrRuO_3$ multi-layer epitaxial thin film electrodes

Kota Suzuki, Kyungsu Kim, Sou Taminato, Masaaki Hirayama, Ryoji Kanno*

Department of Electronic Chemistry, Interdisciplinary Graduate School of Science and Engineering, Tokyo Institute of Technology, 4259 Nagatsuta-cho, Midori-ku, Yokohama 226-8502, Japan

HIGHLIGHTS

- Multi-layer $LiMn_2O_4/SrRuO_3$ epitaxial film electrode was successfully fabricated.
- $SrRuO_3$ as an electronic conducting buffer layer improved electrochemical property.
- No effects on the $LiMn_2O_4$ structure with the stacking of the buffer layer.
- Electrochemical property depends on an electronic contact of the substrate/electrode.

ARTICLE INFO

Article history:
Received 29 October 2012
Accepted 7 November 2012
Available online 13 November 2012

Keywords:
Epitaxial thin film
Lithium manganese oxide
Buffer layer
Lithium battery
Multi-layer electrode

ABSTRACT

Multi-layer thin films of $LiMn_2O_4/SrRuO_3$ have been epitaxially grown on $SrTiO_3$ (111) substrates using a pulsed laser deposition method. The multi-layer electrodes show excellent electrochemical properties due to introduction of an electronic conducting buffer layer between the lithium cathode film and semiconducting substrate. Moreover, the electrochemical characteristics of the lithium cathode materials are strongly dependent on the electronic contact. Thus, the epitaxially grown electrodes can be used as ideal crystalline models to obtain information about the lattice plane, surface roughness, and thickness of electrodes. This information can be used to elucidate the reaction mechanisms of lithium batteries.

1. Introduction

In order to develop next-generation lithium batteries, it is important to understand their reactions. Recently, epitaxially grown thin films have been developed as model electrode systems to clarify the reactions at the electrochemical interface [1–8]. The model systems have provided new insights into lithium battery reactions. These epitaxial model electrodes provide a simple two-dimensional reaction field due to their flat surface with a roughness of less than 1 nm, thus enabling continuous surface structural changes to be detected by *in situ* surface X-ray and neutron scattering techniques [1–8]. In addition, the thin film electrodes have a unitary crystal plane parallel to the interface between the electrodes and the electrolyte due to the presence of single crystal substrates, thus providing novel information about the lattice plane dependence on (de)intercalation mechanisms as well as information about the surface stability [1–6,8].

However, the electrochemical properties of these epitaxial model systems have not been well characterized, although *in situ* or *ex situ* experimental measurements of structure changes due to electrochemical reactions provide atomistic information about the interfacial region. This might be due to an electric contact between the semiconducting substrate and semiconducting electrode used for the lithium battery reaction. For example, the theoretical capacity of $LiMn_2O_4$ could not be obtained for the epitaxial film electrode. Unfavorable effects due to the single crystal substrates could affect the electrochemical properties of the $LiMn_2O_4$ thin film electrodes. This might be due to a strain caused by the substrate, which affects the structural changes and phase transitions [9–11], thus decreasing its electrochemical response by lithium (de)intercalation. Poor electric conduction of the single crystal substrates of Nb-doped $SrTiO_3$ (0.5%Nb, 10 × 10 × 0.5 mm size with a specific electrical resistance of 5.28×10^{-3} Ω cm at room temperature) could prevent charge transfer at the electrochemical interface. Although Nb doping decreases the specific electrical resistance of $SrTiO_3$ (>10^7 Ω cm), its absolute value is quite large compared to metallic substrates (Al: 2.66×10^{-6} Ω cm; Cu: 1.67×10^{-6} Ω cm),

* Corresponding author. Tel./fax: +81 45 924 5401.
E-mail address: kanno@echem.titech.ac.jp (R. Kanno).

0378-7753/$ – see front matter © 2012 Elsevier B.V. All rights reserved.
http://dx.doi.org/10.1016/j.jpowsour.2012.11.008

Table 1
PLD conditions for epitaxial $SrRuO_3$ thin films.

Target	Temperature /°C	Distance /cm	Duration time /min	Energy /mJ	Frequency /Hz	O_2 pressure /Pa
$SrRuO_3$	600–700	6.0–7.0	30–60	80–100	5–10	10
$Li_{1.2}Mn_2O_4$	650	6.0–7.0	30	80–90	10	6.6

which are generally used as current collectors of the electrodes in lithium batteries. A heterojunction between the electrode thin films and $SrTiO_3$ substrates could induce rectification behavior, because both the electrodes and the substrates are semiconductors [12–15]. Side reaction or ionic diffusion between the substrate and electrode during pulsed laser deposition (PLD) synthesis might also be a factor that prevents the electronic conduction.

In the present study, a metallic $SrRuO_3$ film with a perovskite structure was introduced as a buffer layer between the electrodes and substrates. $SrRuO_3$ was chosen due to its small lattice mismatch with the $SrTiO_3$ substrate, its metallic conductivity of $<10^{-3}$ Ω cm and easiness to grow its thin film with an atomically ideal flat surface [11,16–18]. Consequently, the same epitaxial growth conditions as the $SrTiO_3$ substrate for lithium battery thin film electrodes can be used. Multi-layered electrodes, $LiMn_2O_4/SrRuO_3$, were synthesized on $SrTiO_3$ (111) substrates, and their electrochemical properties were clarified.

2. Experimental

PLD conditions for the synthesis of a $SrRuO_3$ thin film and the properties of the film as a buffer layer have been reported [19–21]. $LiMn_2O_4/SrRuO_3$ multi-layer thin films were grown on $SrTiO_3$ (111) substrates using a KrF excimer laser with a wavelength of 248 nm and PLD apparatuses (PLAD131, AOV Inc. and PLD 3000, PVD Products, Inc.). The substrates were washed with ultra pure water and annealed at 1000 °C under oxygen gas flow. After the annealing treatment, gold deposition was carried out for both the back and lateral sides of the substrates using a QUICK COATER SC-701 (Sanyu Electron Co., Ltd.). A sintered $SrRuO_3$ (Toshima Manufacturing Co., Ltd.) was used as the PLD target. The synthesis conditions of the PLD target for $LiMn_2O_4$ deposition have been described elsewhere [3]. Table 1 summarizes the synthesis conditions for the PLD deposition of each layer. After the $SrRuO_3$ deposition, the substrates were cooled down to room temperature. Then, the substrates were reheated to 650 °C for the next $LiMn_2O_4$ deposition. The entire process for multi stacking was performed in a vacuum chamber to avoid surface contamination of the $SrRuO_3$ buffer layer [22,23]. The surface morphology and roughness of the $SrRuO_3$ were investigated by atomic force microscopy (AFM, JSPM-5200, JEOL Ltd.). Orientations and thicknesses of the films were characterized by X-ray diffraction (XRD) and X-ray reflectometry (XRR) using a thin-film X-ray diffractometer (ATX-G, Rigaku) with Cu $K\alpha_1$ radiation. XRR results were analyzed using the Parratt32 software to evaluate the thickness, density and roughness of each layer.

Electrochemical characterizations were performed using a two-electrode configuration. Cells were assembled inside an argon-filled glove box with lithium metal as the counter electrode and the $LiMn_2O_4/SrRuO_3$ thin films as the working electrode. Ethylene carbonate (EC)/diethyl carbonate (DEC) with a molar ratio of 3:7 was employed as a solvent and a supporting electrolyte of 1 M $LiPF_6$. Cyclic voltammetry (CV) was carried out using a potentio/galvanostat (CompactStat, IVIUM). Galvanostatic charge-discharge

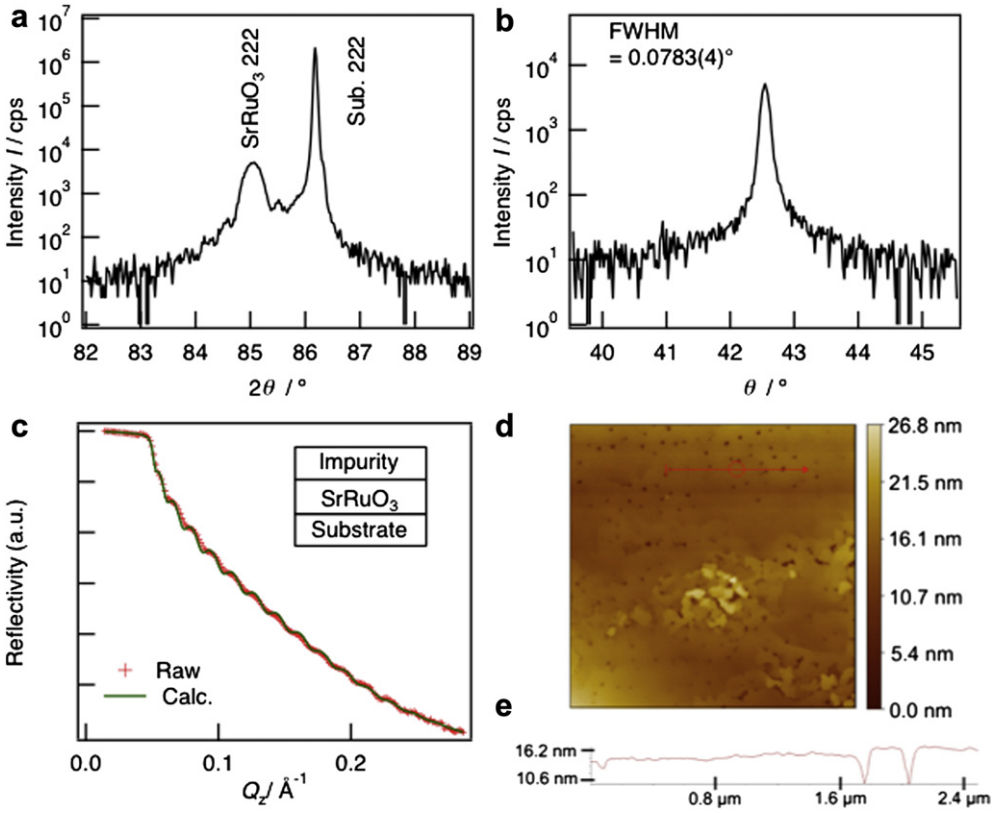

Fig. 1. XRD patterns for the $SrRuO_3$ thin film, (a) out-of-plane and (b) rocking curve of the 222 reflection. (c) XRR spectra with the fitting curve for the $SrRuO_3$ thin film. The inset illustrates the three-layer fitting model for the XRR simulation. (d) AFM image of a 5 × 5 μm^2 area for the $SrRuO_3$ thin film with a thickness of 33 nm. (e) Line profile along the red arrow shown in the AFM image. (For interpretation of the references to color in this figure legend, the reader is referred to the web version of this article.)

Table 2
XRR analysis results for $SrRuO_3$ thin film.

Surface layer			$SrRuO_3$			Substrate	χ^2
t/nm	d/g cm^{-3}	r/nm	t/nm	d/g cm^{-3}	r/nm	r/nm	$(\log(R_{exp})-\log(R_{fit}))^2$
1.75	5.80	0.73	32.8	6.33	0.22	1.19	0.0021

measurements were performed after the CV measurement. A constant current at a rate of 0.64 C was applied for the charged or discharged conditions at 25 °C without any holding time.

3. Results and discussion

3.1. Characterization of $SrRuO_3$ buffer layer

The $SrRuO_3$ buffer layers were characterized by XRD and XRR. Fig. 1(a) shows the out-of-plane XRD pattern of the $SrRuO_3$ thin film deposited on the $SrTiO_3$ substrate at an energy of 100 mJ for a duration time of 30 min. The observed diffraction peaks of the $SrRuO_3$ film are indexed using a pseudo cubic unit cell [23]. The film shows the 222 diffraction line, indicating a (111) orientation of the $SrRuO_3$ on the $SrTiO_3$ (111). The lattice parameter of a pseudo cubic lattice calculated by the 222 diffraction is 3.948 Å, indicating formation of a perovskite structure with a slightly larger unit cell than the $SrTiO_3$ substrate (a = 3.901 Å). Pendellösung interference fringes are observed in the out-of-plane XRD pattern around the 222 diffraction peak of the film. These fringes are usually observed when thin films have strong orientation characteristics [11,24,25]. The fringes in the diffraction peaks show a highly oriented character of the $SrRuO_3$ buffer layer.

In the in-plane XRD pattern along the [1–10] direction of the substrate, no diffraction line attributed to the $SrRuO_3$ structure is observed. This indicates that the $SrRuO_3$ thin film has a similar lattice parameter to that of the substrate (a = 3.901 Å) along the [1–10] direction. The XRD pattern for the rocking curve of the 222 reflection in Fig. 1(b) shows a sharp diffraction peak with a full width at a half maximum value of 0.0783°. The deposited $SrRuO_3$ thin films have a highly oriented character in both the perpendicular and horizontal directions. The lattice volume is calculated to be 60.1 Å^3 based on the lattice parameters of 3.948 Å and 3.901 Å for the out-of-plane and in-plane directions, respectively. This value is in good agreement with the stoichiometric $SrRuO_3$ epitaxial thin films with metallic behavior and a small resistivity of $<2 \times 10^{-6}$ Ω cm at 300 K [26].

Fig. 1(c) shows the XRR spectra of both the observed and calculated curves. These spectra are plotted as a function of the scattering vector $q = 4\pi \sin\theta/\lambda$, where λ is the X-ray wavelength (1.541 Å) and θ is the incident angle. A three-layer model was applied for the fitting of the XRR spectra to take into account the formation of the impurity layer [27,28]. Table 2 summarizes the refined parameters of each layer, thickness: t, density: d and roughness: r. The density and thickness of the $SrTiO_3$ substrate were fixed as 5.12 g cm^{-3} and 0.5 mm, respectively. A surface impurity layer with a density of ρ = 5.80 g cm^{-3} could be attributed to Sr_2RuO_4 (ρ = 5.75–5.96 g cm^{-3}). The roughness values of the impurity layer and the $SrRuO_3$ thin film are determined to be 0.73

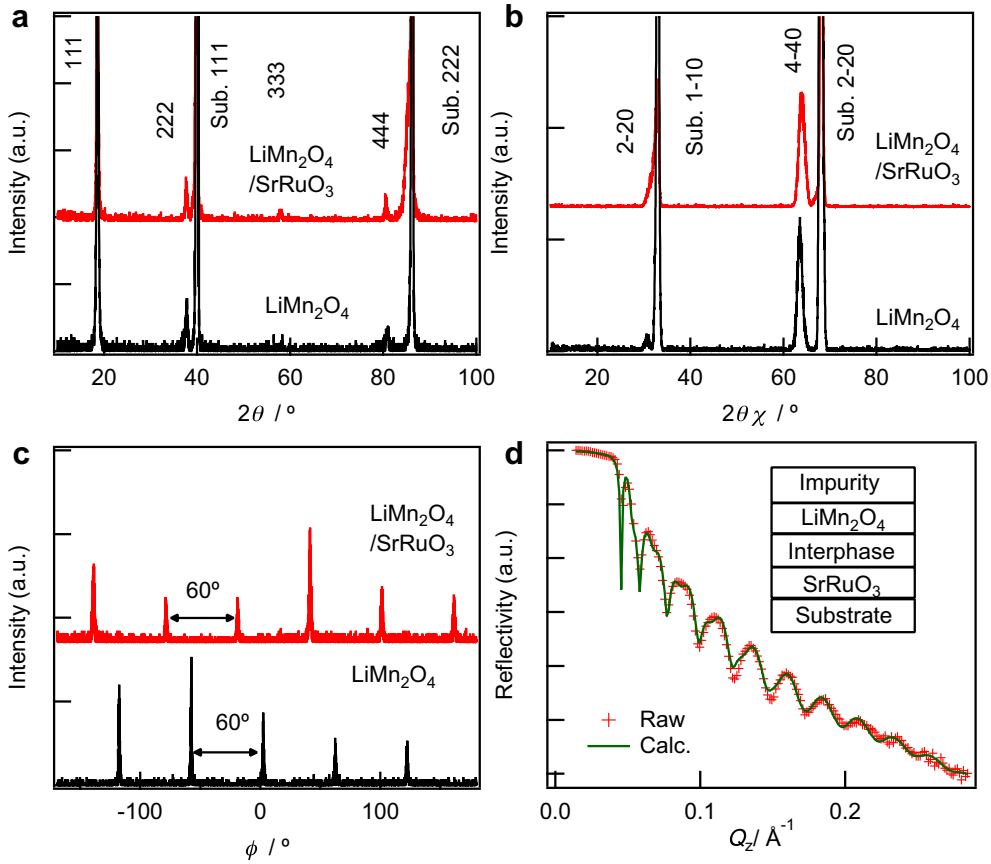

Fig. 2. XRD patterns for the $LiMn_2O_4$ epitaxial thin film electrodes, (a) out-of-plane and (b) in-plane along the [1–10] direction of the substrate. (c) φ scan XRD patterns of the 4–40 reflection of the spinel. Red and black lines are attributed to the $LiMn_2O_4/SrRuO_3$ and the $LiMn_2O_4$, respectively. (d) XRR spectrum and fitting curve for the $LiMn_2O_4/SrRuO_3$. The inset shows the simulation model. (For interpretation of the references to color in this figure legend, the reader is referred to the web version of this article.)

and 0.22 nm, respectively. The flat surface could enhance the formation of smooth $LiMn_2O_4$ films on the buffer layer. The thickness of the $SrRuO_3$ is controlled from 5 to 50 nm without any significant changes in the roughness and the density by changing the duration time and laser energy of the PLD conditions.

The AFM image is shown in Fig. 1(d). Although an ideal step with a terrace structure is not observed, a large flat area in micrometer order is confirmed. Fig. 1(e) shows the line profile of the voids at the flat region of the $SrRuO_3$ buffer layer. The difference in height between the surface of the buffer layer and the hollow point is about 5 nm. The surface morphology observed indicate that $SrRuO_3$ is suitable as a buffer layer of $LiMn_2O_4$ electrodes.

3.2. Characterization of $LiMn_2O_4/SrRuO_3$ multi-layer film

$LiMn_2O_4$ and $LiMn_2O_4/SrRuO_3$ epitaxial thin films were deposited on the $SrTiO_3$ (111) substrates without exposure to ambient air using the same PLD conditions. Fig. 2(a,b) shows the respective out-of-plane and in-plane [1–10] XRD patterns of the $LiMn_2O_4$ and $LiMn_2O_4/SrRuO_3$ films deposited on the $SrTiO_3$ (111). Both films show 111, 222, 333 and 444 diffraction lines, indicating a (111) orientation of the $LiMn_2O_4$ films on the $SrTiO_3$ (111). The lattice parameter of the spinel is calculated to be 8.253 and 8.225 Å for $LiMn_2O_4$ and $LiMn_2O_4/SrRuO_3$, respectively. The parameter slightly increases along the [111] direction when the buffer layer is introduced. The $LiMn_2O_4$ of both films shows the [1–10] orientation along the in-plane [1–10] direction of the $SrTiO_3$ substrate. The epitaxial $LiMn_2O_4$ films are successfully synthesized on the $SrRuO_3$ buffer layer [3,6]. The lattice parameter of 8.229 Å calculated from the 4–40 diffraction peak of the spinel in $LiMn_2O_4/SrRuO_3$ is slightly smaller than the parameter along the [111] direction, indicating an anisotropic strain due to the substrate. However, the difference of the lattice parameter of the spinel in $LiMn_2O_4/SrRuO_3$ between the [111] and [1–10] directions is 0.024 Å, which is smaller than that of the spinel in $LiMn_2O_4$ (0.049 Å) without the buffer layer. The $SrRuO_3$ buffer layer reduces the strain of lattice mismatch between the $LiMn_2O_4$ and $SrTiO_3$ substrate. Out-of-plane and in-plane measurements indicate that the $LiMn_2O_4$ thin film is slightly distorted from the ideal cubic spinel structure. To confirm the symmetry, the φ scan was measured with a fixed $2\theta\chi$ value for the 4–40 reflection. Fig. 2(c) shows the XRD patterns for the φ scan of the $LiMn_2O_4$ and the $LiMn_2O_4/SrRuO_3$. Six diffraction peaks at an interval of 60° indicate a sixfold symmetry of $LiMn_2O_4$ along the [111] direction for both films.

Fig. 2(d) shows the observed and calculated XRR spectra of the $LiMn_2O_4/SrRuO_3$ thin films. Table 3 summarizes the refined parameters, thickness: t, density: d and roughness: r, of each layer. The residual sum of squares for $LiMn_2O_4/SrRuO_3$ (0.0230) is higher than that for $LiMn_2O_4$ (0.0021) due to a multi-layer character. The reflectivity data confirms the existence of the impurity layer with a density of 2.11–2.14 g cm^{-3}, which may be due to Li_2CO_3 ($\rho = 2.1$ g cm^{-3}) or LiOH ($\rho = 1.5$ g cm^{-3}) [1–3,7]. A formation of the interphase layer with a density of 4.39–4.55 g cm^{-3} is also confirmed between the $LiMn_2O_4$ and $SrRuO_3$. The $LiMn_2O_4/SrRuO_3$ film shows a small roughness of about 1 nm, which is comparable to that of $LiMn_2O_4$. There is no significant difference in the density of the spinel between the $LiMn_2O_4/SrRuO_3$ and the $LiMn_2O_4$, and the density value is in good agreement with the theoretical value of $LiMn_2O_4$ ($\rho = 4.28$ g cm^{-3}). To summarize the structures of the multi-layer film, no differences in thickness, density and roughness are observed for the spinel between $LiMn_2O_4$ and $LiMn_2O_4/SrRuO_3$ films. The multi-layer thin films deposited on the $SrTiO_3$ (111) are suitable as model electrodes [1–8].

Table 3
XRR analysis results for the (a) $LiMn_2O_4/SrRuO_3$ and (b) $LiMn_2O_4$ thin films.

		t/nm	d/g cm^{-3}	r/nm
(a)	Impurity	1.2	2.14	0.51
	$LiMn_2O_4$	21.0	4.30	1.20
	Interphase	2.9	4.55	1.91
	$SrRuO_3$	26.4	6.31	0.99
	Substrate	–	–	1.50
(b)	Impurity	1.0	2.11	0.52
	$LiMn_2O_4$	20.1	4.29	0.80
	Substrate	–	–	0.82

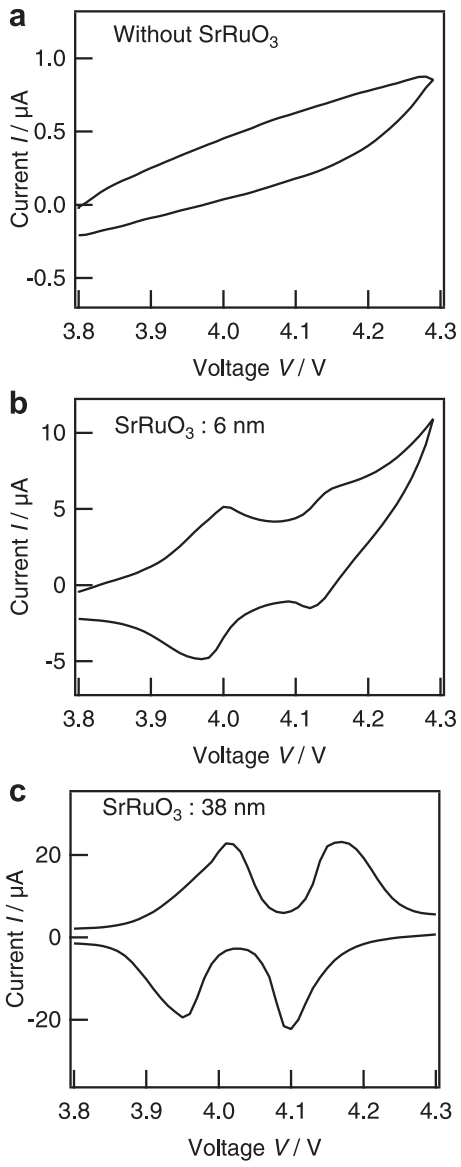

Fig. 3. CV curves for the $LiMn_2O_4$ thin film electrodes, (a) $LiMn_2O_4$(22 nm), (b) $LiMn_2O_4$(22 nm)/$SrRuO_3$(6 nm) and (c) $LiMn_2O_4$(33 nm)/$SrRuO_3$(38 nm). Scan rates of the measurements were (a) 5 mV s^{-1}, (b) 5 mV s^{-1} and (c) 1 mV s^{-1}.

3.3. Electrochemical properties of $LiMn_2O_4/SrRuO_3$ multi-layer film

Fig. 3 shows the CV curve of the $LiMn_2O_4$ and $LiMn_2O_4/SrRuO_3$ electrodes. The CV curve of $LiMn_2O_4$(22 nm) shows no redox peaks in cathodic and anodic scans with passing currents below 1.0 μA. On the other hand, the $LiMn_2O_4/SrRuO_3$ electrodes show redox

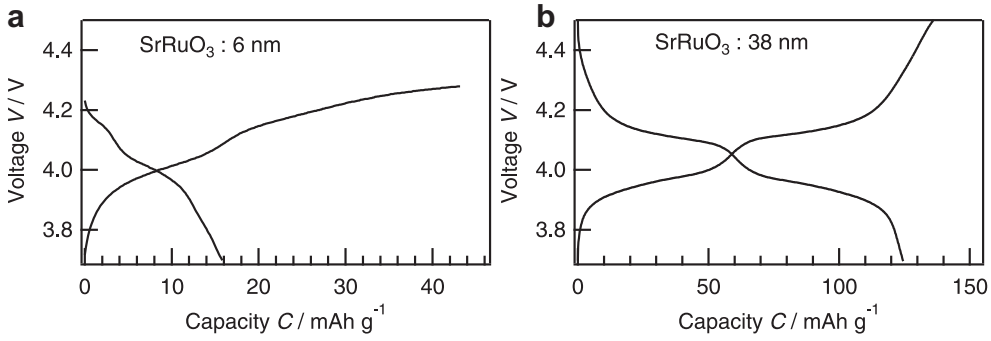

Fig. 4. Charge-discharge curves for (a) $LiMn_2O_4$(22 nm)/$SrRuO_3$(6 nm) and (b) $LiMn_2O_4$(33 nm)/$SrRuO_3$(38 nm).

peaks around 4.0 and 4.1 V. Oxidation and reduction peaks are observed around 4.0 and 4.1 V in the cathodic and anodic scans, which are attributed to the lithium extraction and insertion reaction, respectively [29,30]. The $SrRuO_3$ buffer layer enhances the electrochemical properties of the $LiMn_2O_4$ epitaxial thin film electrodes. Because no significant differences in thickness, density and roughness are observed between both films, the enhancement of the electrochemical properties is attributed to the change in electronic connection at the semiconducting substrate and semiconducting electrode. Furthermore, the interphase formed at the electrode/buffer layer interface does not affect the electrochemical property. The $LiMn_2O_4$(33 nm)/$SrRuO_3$(38 nm) shows clear redox peaks with a current four times as large as that of the $LiMn_2O_4$(22 nm)/$SrRuO_3$(6 nm). The thickness of the buffer layer affects the electrochemical properties of the $LiMn_2O_4$ electrode.

The $LiMn_2O_4/SrRuO_3$ multi-layer film electrodes were subjected to a charge-discharge test after the CV measurement. Fig. 4 shows the charge-discharge curves of the multi-layer film electrodes. The specific capacities of the multi-layer electrodes were calculated based on the amount of the $LiMn_2O_4$ defined by the area (0.9 mm^2), density (4.28 g cm^{-3}) and thickness (22 or 33 nm). The $LiMn_2O_4$(22 nm)/$SrRuO_3$(6 nm) shows a small charge capacity of 44 mAh g^{-1} (theoretical capacity 148 mAh g^{-1}), with (i) no plateau regions corresponding to the lithium (de)intercalation, (ii) different shapes between the charge and discharge curves, and (ii) a large irreversible capacity of 26 mAh g^{-1} which corresponds to 60% of the charge capacity. On the other hand, the $LiMn_2O_4$(33 nm)/$SrRuO_3$(38 nm) shows a discharge capacity of 125 mAh g^{-1} with a small irreversible capacity of 10 mAh g^{-1}, with clear plateau regions in the charge and discharge processes. Excellent electrochemical properties are observed for thicker buffer layers. The electrochemical property depends on the thickness of the metallic buffer layer, and a thicker film is necessary for good electrochemical characteristics. To summarize, excellent electrochemical properties are observed for the epitaxial $LiMn_2O_4$ thin film electrode using $LiMn_2O_4/SrRuO_3$ multi-layer compositions with the 38 nm-thick buffer layer.

4. Conclusion

$LiMn_2O_4/SrRuO_3$ multi-layer epitaxial thin film electrodes were successfully synthesized on $SrTiO_3$ (111) by the PLD method. The $SrRuO_3$ (111) buffer layers showed a highly oriented and notable flat surface, which could provide a suitable bottom field for the epitaxial growth of the $LiMn_2O_4$ epitaxial thin films. No significant degradation was observed for the quality of the epitaxial $LiMn_2O_4$ thin film electrodes deposited on the buffer layer, compared to the direct deposition on the $SrTiO_3$ substrate. Obtained multi-layer electrodes provide not only a restricted reaction field suitable for mechanistic studies of the interfacial reactions, but also enhance the electrochemical properties of the electrodes. As a result, their detailed reaction mechanism is worth discussing. Lithium (de) intercalation through the (111) plane of the $LiMn_2O_4$ electrodes was confirmed by the electrochemical techniques, cyclic voltammetry and charge-discharge measurements.

Acknowledgments

The authors would like to thank Dr. Shimakawa (University of Kyoto) for his valuable comments. This work was conducted as part of a collaboration program with the Genesis Research Institute. This work was partly supported by a Grant-in-Aid for Scientific Research (A), a Grant-in-Aid for Young Scientists (B), a Grant-in-Aid for Japan Society for the Promotion of Science (JSPS) Fellows, and a Grant-in-Aid for Advanced Low Carbon Technology Research and Development Program (ALCA) in Japan Science and Technology Agency (JST).

References

[1] M. Hirayama, K. Sakamoto, T. Hiraide, D. Mori, A. Yamada, R. Kanno, N. Sonoyama, K. Tamura, J. Mizuki, Electrochim. Acta 53 (2007) 871–881.
[2] M. Hirayama, N. Sonoyama, T. Abe, M. Minoura, M. Ito, D. Mori, A. Yamada, R. Kanno, T. Terashima, M. Takano, K. Tamura, J. Mizuki, J. Power Sources 168 (2007) 493–500.
[3] M. Hirayama, N. Sonoyama, M. Ito, M. Minoura, D. Mori, A. Yamada, K. Tamura, J. Mizuki, R. Kanno, J. Electrochem. Soc. 154 (2007) A1065–A1072.
[4] K. Sakamoto, H. Konishi, N. Sonoyama, A. Yamada, K. Tamura, J. Mizuki, R. Kanno, J. Power Sources 174 (2007) 678–682.
[5] K. Sakamoto, M. Hirayama, N. Sonoyama, D. Mori, A. Yamada, K. Tamura, J. Mizuki, R. Kanno, Chem. Mater. 21 (2009) 2632–2640.
[6] M. Hirayama, H. Ido, K. Kim, W. Cho, K. Tamura, J. Mizuki, R. Kanno, J. Am. Chem. Soc. 132 (2010) 15268–15276.
[7] M. Hirayama, M. Yonemura, K. Suzuki, N. Torikai, H. Smith, E. Watkinsand, J. Majewski, R. Kanno, Electrochemistry 78 (2010) 413–415.
[8] K. Sakamoto, M. Hirayama, H. Konishi, N. Sonoyama, N. Dupre, D. Guyomard, K. Tamura, J. Mizuki, R. Kanno, Phys. Chem. Chem. Phys. 12 (2010) 3815–3823.
[9] F. He, B.O. Wells, Z.G. Ban, S.P. Alpay, S. Grenier, S.M. Shapiro, W. Si, A. Clark, X.X. Xi, Phys. Rev. B. 70 (2004) 235405.
[10] A. Tebano, C. Aruta, P.G. Medaglia, F. Tozzi, G. Balestrino, A.A. Sidorenko, G. Allodi, R. De Renzi, G. Ghiringhelli, C. Dallera, L. Braicovich, N.B. Brookes, Phys. Rev. B. 74 (2006) 245116.
[11] K.J. Choi, S.H. Baek, H.W. Jang, L.J. Belenky, M. Lyubchenko, C.-B. Eom, Adv. Mater. 22 (2010) 759–762.
[12] Y. Watanabe, Phys. Rev. B. 57 (1998) R5563–R5566.
[13] Y. Watanabe, Phys. Rev. B. 59 (1999) 11257–11266.
[14] F.X. Hu, J. Gao, J.R. Sun, B.G. Shen, Appl. Phys. Lett. 83 (2003) 1869–1871.
[15] P. Han, K.-j. Jin, H.-b. Lu, Q.-L. Zhou, Y.-L. Zhou, G.-Z. Yang, Appl. Phys. Lett. 91 (2007) 182102–182103.
[16] J. Chang, Y.S. Park, J.W. Lee, S.K. Kim, J. Cryst, Growth 311 (2009) 3771–3774.
[17] D. Toyota, I. Ohkubo, H. Kumigashira, M. Oshima, T. Ohnishi, M. Lippmaa, M. Takizawa, A. Fujimori, K. Ono, M. Kawasaki, H. Koinuma, Appl. Phys. Lett. 87 (2005) 162508.
[18] D. Kan, Y. Shimakawa, J. Appl. Phys. 111 (2012) 093532–093535.
[19] Q.X. Jia, X.D. Wu, S.R. Foltyn, P. Tiwari, Appl. Phys. Lett. 66 (1995) 2197–2199.

[20] C.H. Ahn, T. Tybell, L. Antognazza, K. Char, R.H. Hammond, M.R. Beasley, ò. Fischer, J.M. Triscone, Science 276 (1997) 1100–1103.
[21] J. Choi, C.B. Eom, G. Rijnders, H. Rogalla, D.H.A. Blank, Appl. Phys. Lett. 79 (2001) 1447–1449.
[22] J. Shin, S.V. Kalinin, H.N. Lee, H.M. Christen, R.G. Moore, E.W. Plummer, A.P. Baddorf, J. Mater. Res. 19 (2004) 3447–3450.
[23] A. Ito, H. Masumoto, T. Goto, S. Sato, J. Eur. Ceram. Soc. 30 (2010) 435–440.
[24] D. Rubi, A.H.G. Vlooswijk, B. Noheda, Thin Solid Films 517 (2009) 1904–1907.
[25] H. Ohta, T. Mizoguchi, N. Aoki, T. Yamamoto, A. Sabarudin, T. Umemura, Appl. Phys. Lett. 100 (2012) 173107.
[26] T. Ohnishi, K. Takada, Appl. Phys. Express 4 (2011) 025501.
[27] J. Shin, S.V. Kalinin, H.N. Lee, H.M. Christen, R.G. Moore, E.W. Plummer, A.P. Baddorf, Surf. Sci. 581 (2005) 118–132.
[28] C. Mallika, O.M. Sreedharan, J. Alloys Compd. 191 (1993) 219–222.
[29] X. Sun, X.Q. Yang, M. Balasubramanian, J. McBreen, Y. Xia, T. Sakai, J. Electrochem. Soc. 149 (2002) A842–A848.
[30] R.J. Gummow, A. de Kock, M.M. Thackeray, Solid State Ionics 69 (1994) 59–67.